



1 Surface wave tomography of China from ambient seismic 2 noise correlation

3 **Sihua Zheng**

4 *Institute of Earthquake Science, China Earthquake Administration, No. 63, Fuxing Avenue, Beijing, 100036, China*

6 *Department of Geology, University of Illinois, 1301 West Green Street, 245 NHB, Urbana, Illinois 61891, USA*

7 **Xinlei Sun and Xiaodong Song**

8 *Department of Geology, University of Illinois, 1301 West Green Street, 245 NHB, Urbana, Illinois 61891, USA*

9 *(xsong@uiuc.edu)*

10 **Yingjie Yang and Michael H. Ritzwoller**

11 *Department of Physics, University of Colorado at Boulder, Campus Box 390, Boulder 80309, Colorado, USA*

12 [1] We perform ambient noise tomography of China using data from the China National Seismic Network
13 and surrounding global and regional stations. For most of the station pairs, we retrieve good Rayleigh
14 waveforms from ambient noise correlations using 18 months of continuous data at all distance ranges
15 across the entire region (over 5000 km) and for periods from 70 s down to about 8 s. We obtain Rayleigh
16 wave group velocity dispersion measurements using a frequency-time analysis method and invert for
17 Rayleigh wave group velocity maps for periods from 8 s to 60 s. The tomographic maps display significant
18 features that correlate with surface geology. Major basins, including Tarim, Junggar, Qadaim, Sichuan,
19 Bohai-Wan, and Songliao, are all well delineated by slow group velocities at shorter periods (10 to 20 s).
20 The overall trend of crustal thickening from east to west is well represented by group velocity decreases
21 from east to west at periods around 30 s.

22 **Components:** 3888 words, 7 figures.

23 **Keywords:** surface wave; tomography; ambient noise correlation; China.

24 **Index Terms:** 7255 Seismology: Surface waves and free oscillations; 7270 Seismology: Tomography (6982, 8180);
25 7205 Seismology: Continental crust (1219).

26 **Received** 5 February 2008; **Revised** 18 March 2008; **Accepted** 26 March 2008; **Published** XX Month 2008.

27 Zheng, S., X. Sun, X. Song, Y. Yang, and M. H. Ritzwoller (2008), Surface wave tomography of China from ambient seismic
28 noise correlation, *Geochem. Geophys. Geosyst.*, 9, XXXXXX, doi:10.1029/2008GC001981.

30 1. Introduction

31 [2] Recent theoretical and laboratory studies have
32 shown that the Green functions of a structure can
33 be obtained from the cross correlation of diffuse
34 wavefields [e.g., *Lobkis and Weaver, 2001*] (see

also review by *Campillo [2006]*). The basic idea is 35
that linear waves preserve, regardless of scattering, 36
a residual coherence that can be stacked and 37
amplified to extract coherent information between 38
receivers [e.g., *Weaver, 2005*]. The idea has now 39
found rapid applications in seismology. In particu- 40

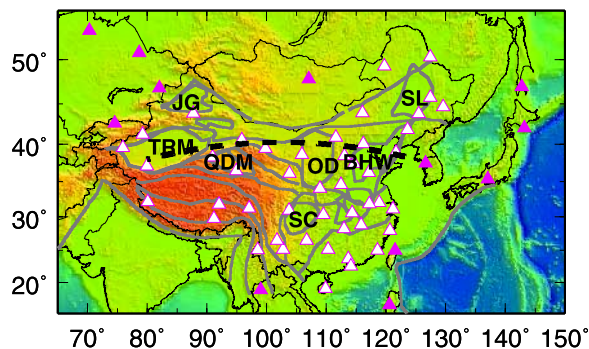


Figure 1. Distribution of seismic stations used in this study, including China National Seismic Network (CNSN) stations (open triangles) and stations in the surrounding regions (solid triangles). Plotted also are major tectonic boundaries [from Liang *et al.*, 2004] and major basins. The basins that are labeled include Tarim (TRM), Junggar (JG), Qaidam (QD), Sichuan (SC), Ordos (OD), Bohai Wan (BHW), and Songliao (SL) basins. The thick dashed line across northern China from the Tarim Basin to Korea indicates the selected great circle path for Figure 6.

studies of the region have relied on a sparse network of the Chinese Digital Seismic Network (CDSN) (with 10 stations) established in 1986 and other global stations in adjacent regions [e.g., Zhang and Lay, 1996; Wu *et al.*, 1997; Ritzwoller and Levshin, 1998; Curtis *et al.*, 1998; Xu *et al.*, 2000; Zhu *et al.*, 2002; Huang *et al.*, 2003; Lebedev and Nolet, 2003; Yao *et al.*, 2005]. The surface wave periods range from about 10 s up to 250 s. Here we obtain inter-station dispersion measurements and perform ANT of China using stations from the new China National Seismic Network (CNSN) and a few stations in the surrounding regions (Figure 1). The CNSN is the national backbone network, established around 2000, with a relatively uniform distribution across the continental China. We focus on Rayleigh wave group velocities in this study. The dispersion measurements and tomographic maps provide a brand new and complementary data set critically needed for constraining the 3-D structure of the region.

2. Data and Method

[5] We use 18 months of continuous data from 47 CNSN stations and 12 other stations. All stations are broadband. The bandwidths of the CNSN stations are from 20 Hz to at least 120 s. We use the data processing and imaging techniques described in detail by Bensen *et al.* [2007]. To avoid the redundancy we summarize our data processing only briefly below.

[6] We first obtain the empirical Green function (EGF) from ambient noise cross correlation. Continuous data are pre-processed before correlation and stacking, which includes clock synchronization, removal of instrument response, time domain filtering, temporal normalization and spectral whitening. The purpose is to reduce the influence of earthquake signals and instrument irregularities and to enhance the strength and bandwidth of the ambient noise correlations. In particular, we follow Bensen *et al.* [2007] and perform time domain normalization, which normalizes the time series by a running average. The running average is computed between 15 and 25 s period, a band in which small earthquakes are typically stronger than microseismic noise. Bensen tested it versus sign bit normalization and found it superior in the presence of numerous small earthquakes within the seismic array. Cross correlations are done daily and then stacked over all time periods (18 months). All the processes are linear, so breaking the cross correla-

lar, surface waves have been found to be most easily retrievable from the cross correlations of seismic coda [Campillo and Paul, 2003; Paul *et al.*, 2005] or ambient noise [Shapiro and Campillo, 2004; Shapiro *et al.*, 2005; Sabra *et al.*, 2005a, 2005b] between two stations. Both Rayleigh waves and Love waves can be retrieved. The new type of data has rapidly been used for tomographic mapping at regional or local scales [e.g., Shapiro *et al.*, 2005; Sabra *et al.*, 2005b; Kang and Shin, 2006; Villaseñor *et al.*, 2007; Liang and Langston, 2008] and on continental scales [e.g., Yang *et al.*, 2007; Bensen *et al.*, 2008]. These studies have focused on Rayleigh wave group velocity tomography from ambient noise. However, the method has been demonstrated to be applicable to Love waves [Lin *et al.*, 2008] and phase velocity measurements [Yao *et al.*, 2006; Lin *et al.*, 2008].

[3] Ambient noise tomography (ANT) overcomes several important limitations of conventional methods based on earthquakes, i.e., uneven distribution of earthquake sources, uncertainty in earthquake location, and attenuation of short-period surface waves. Thus, the method is particularly useful for surface-wave path calibration and for tomographic mapping in aseismic regions especially at short periods (below 30 s).

[4] In this study, we applied the ANT techniques to China. Prior surface wave dispersion and inversion

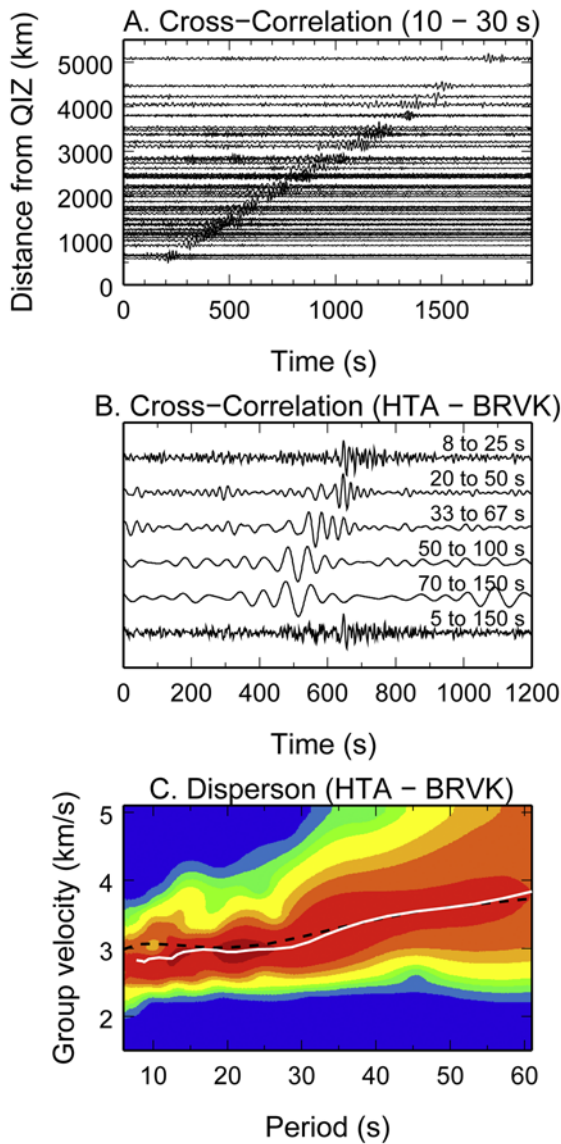


Figure 2. Example of Rayleigh wave EGFs and dispersion measurements obtained from ambient noise correlations. (a) Symmetric component of the correlations between station QIZ (in Hainan Province, China) and other stations. The traces are band pass filtered at relatively short periods (10–30 s). (b) EGFs filtered in different frequency bands. Long-period surface waves are clearly faster than short-period ones. The path is between HTA (bordering Tarim in the south) and BRVK (Borovoye, Kazakhstan). (c) Frequency-time analysis [Ritzwoller and Levshin, 1998] used to retrieve Rayleigh wave group velocity dispersion curve (white) for the HTA-BRVK path. The black dashed curve is the prediction from the 3-D global shear velocity model of Shapiro and Ritzwoller [2002], which is used for phase-matched filtering in the data analysis and for comparison with measurements.

tion into daily procedures, rather than performing 122
over 1.5 yearlong time series, is merely a book- 123
keeping device. The correlation function is often 124
asymmetric with respect to the positive and the 125
negative delays because of non-uniform distribu- 126
tion of noise sources. We use the symmetric 127
component of the correlation as the EGF by 128
averaging the causal and acausal parts of the 129
correlation. 130

[7] If the signal-to-noise ratio (SNR) is sufficiently 131
large, Rayleigh wave group speeds are then mea- 132
sured using a frequency-time analysis [Ritzwoller 133
and Levshin, 1998]. Finally, the inter-station dis- 134
persion measurements are used to invert for the 135
Rayleigh wave group velocity maps, in exactly the 136
same way as earthquake-based measurements. 137

3. Results 138

[8] For most of the station pairs, we are able to 139
retrieve good Rayleigh wave signals from the 140
ambient noise correlations. Figure 2 shows typical 141
examples of EGFs and group velocity measure- 142
ments of Rayleigh waves retrieved from ambient 143
noise correlations. The cross correlations show 144
strong arrivals at different settings (near the coast 145
or well into the continental interior) and at both 146
relatively low frequencies (20–50 s) and high 147
frequencies (5–20 s). The EGFs can be retrieved 148
over the entire region (at distances of over 5000 km) 149
(Figure 2a). 150

[9] We measured group velocity dispersion curves 151
(Figure 2c) for station pairs with Rayleigh wave 152
SNR > 10. The SNR is defined as the ratio of the 153
peak amplitude of the Rayleigh wave to the root- 154
mean square value of the background. The mea- 155
surement is very stable. Clear dispersion can be 156
commonly observed directly from the EGFs 157
(Figure 2b). We found that the group velocity 158
measurements can extend to periods of 10 s or 159
shorter even for station pairs that are separated over 160
thousands of kilometers. The group velocities of the 161
HTA-BRVK path (Figures 2b and 2c), which sam- 162
ples the Tarim Basin, agree with a global 3-D 163
earthquake-based model [Shapiro and Ritzwoller, 164
2002] at longer periods but differ significantly at 165
short periods (below 30 s). The slow group veloc- 166
ities at short periods are caused by the thick sedi- 167
ments of the Tarim Basin (see discussion below). 168

[10] We have obtained dispersion measurements 169
with SNR > 10 for periods 8 s to 70 s (Figure 3a). 170
The best observed frequency band is 10 to 30 s 171
with over 1000 measurements at each period or a 172

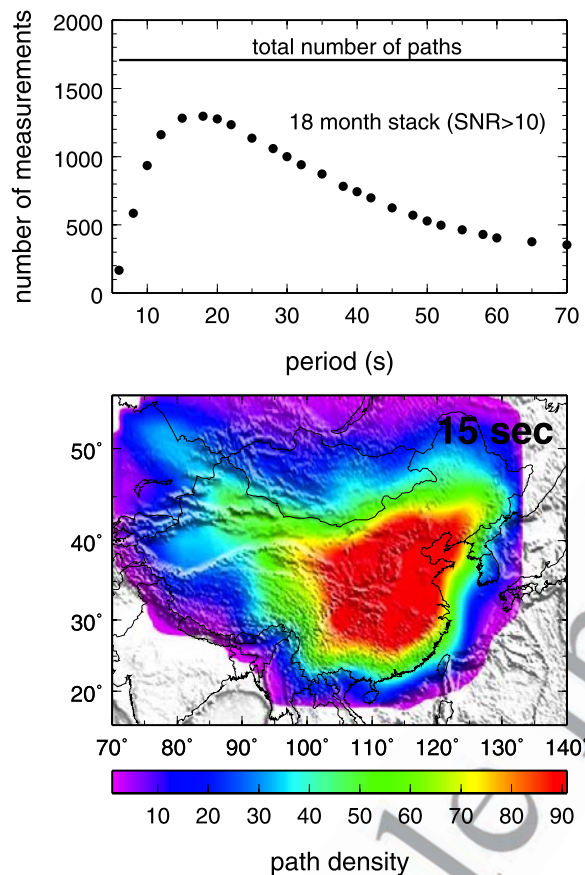


Figure 3. (top) Distribution of dispersion measurements for different periods and (bottom) ray density map for the period of 15 s. (top) The total number of paths takes into account data availability for pairing up stations. (bottom) The ray density is the number of rays inside 1 degree by 1 degree cell. The rays are station pairs for which dispersion measurements have been obtained. The ray coverage is best for periods 10 to 30 s. Coverages for shorter or longer periods deteriorate, but the spatial coverage patterns remain similar.

173 retrieval rate of 50 to 80% of all the possible pairs.
174 The raypaths cover almost the entire continental
175 China (Figure 3b). However, the coverage is much
176 better in the eastern half of the country, because of
177 the denser station distribution there than in the
178 western part.

179 [11] The ray coverage of our dispersion measure-
180 ments is sufficient for us to invert for Rayleigh
181 wave group velocity maps at periods from 8 s to
182 60 s (Figure 4). The results show remarkable
183 features that correlate with large-scale geological
184 structures of China. Major basins are well delin-
185 eated with low velocities at short periods (8 to 20 s),
186 including Bohai-Wan Basin (North China Basin),

Sichuan Basin, Qaidam Basin, and Tarim Basin. 187
The stable Yangtz Craton also shows up well with 188
high velocities. At longer periods (25–50 s), the 189
group velocity maps display striking bimodal dis- 190
tribution with high velocity in the east and low 191
velocity in the west, which corresponds very well 192
with the thinner crust in the east and much thicker 193
crust in the west [e.g., *Liang et al.*, 2004]. The 194
NE-SW trending boundary between fast and 195
slow velocities (around longitude 108°E) coincides 196
with the sharp topographic change and with the 197
well-known Gravity Lineation. 198

[12] A side-by-side comparison between a short 199
period group velocity map and sediment thickness 200
or between an intermediate period map and crustal 201
thickness is presented in Figure 5. The correlations 202
are quite striking if we compare the group veloc- 203
ities along a certain profile of interest (Figure 6). 204
The selected profile along latitude of about 39°N 205
passes through three major basins: Tarim, Ordos, 206
and Bohai-Wan (Figure 1). The thick sediments in 207
these basins [Laske and Masters, 1997] correlate 208
well with slow velocities at periods from 10 to 20 s 209
(Figure 6a). The general trend of decreasing crustal 210
thickness from west to east is well represented by 211
increasing group velocities around 30 s (Figure 6b). 212
However, the group velocity map displays more 213
structure than the smooth crustal thickness curve 214
from the global reference model (CRUST 2.0) 215
(<http://mahi.ucsd.edu/Gabi/rem.html>), suggesting 216
a more complex Moho. At period 50 s, the trend 217
is no longer observable as the surface waves 218
sample deeper into the mantle. 219

4. Conclusion and Discussion 220

[13] Using correlations of 18 months of continuous 221
data from CNSN and global seismic stations, we 222
retrieve Rayleigh wave empirical Green functions 223
(EGFs) over a broad frequency band across China 224
and surroundings. Group velocity dispersion mea- 225
surements are obtained for periods of 8 to 70 s. The 226
best observed frequency band is 10 to 30 s with a 227
retrieval rate of 50 to 80% of the station-pairs. We 228
have constructed Rayleigh wave group velocity 229
maps of China from 8 to 60 s. The tomographic 230
maps show remarkable correlations with the major 231
tectonic features of China, in particular, the major 232
sedimentary basins and crustal thickness. With the 233
rapid growth of digital seismic stations in China, 234
we are hopeful to see much improved tomographic 235
images of the structures of the region in the near 236
future. 237

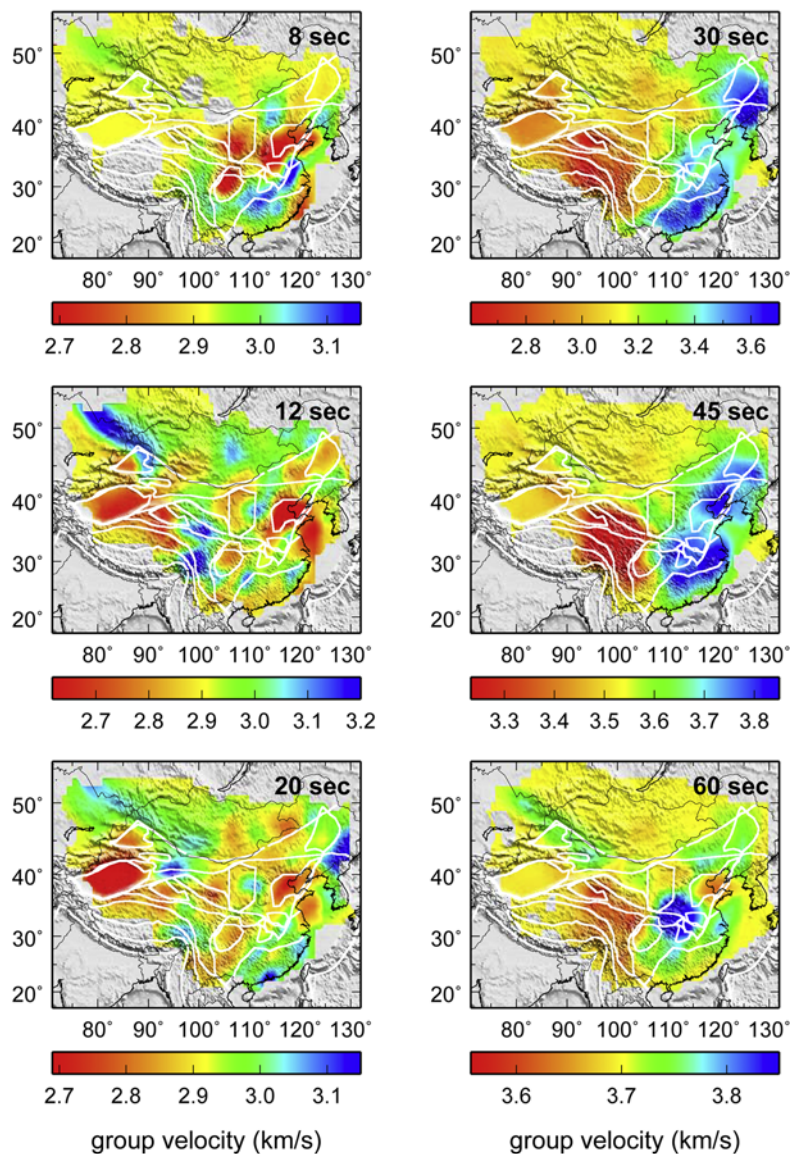


Figure 4. Maps of Rayleigh wave group velocities at periods of 8, 12, 20, 30, 45, and 60 s. Note the color scale for each period is selected so that the scale represents the range of the values with the average value in the middle of the color bar (between yellow and green). The ranges of the values for different periods are different. Plotted in the background are major block boundaries and basin outlines (Figure 1).

238 [14] Comparison of the tomographic maps with the
239 geological features discussed above provides an
240 important initial validation of the ambient noise
241 tomography (ANT) methodology; i.e., the method
242 provides models of group wave speeds that are
243 consistent with well-known geological features and
244 other geophysical observations. Furthermore, the
245 complete repeatability of the ANT method makes it
246 possible to validate directly the methodology and
247 to evaluate the uncertainties of the dispersion
248 measurements. Several methods have been pro-
249 posed in this regard. (1) Direct verification: Com-
250 paring the EGF with the surface wave generated by

an earthquake along the same path [e.g., *Shapiro et al.*, 2005; *Bensen et al.*, 2007]. (2) Comparing the
EGF obtained from ambient noise and that from
seismic coda [*Yao et al.*, 2006]. (3) Temporal
stability: Comparing the EGFs from the data ob-
served at different time periods (e.g., different
months) [*Shapiro et al.*, 2005; *Yao et al.*, 2006;
Bensen et al., 2007]. Furthermore, because the
principal ambient noise sources are believed to
come from the oceans [e.g., *Yang and Ritzwoller*,
2008], which are seasonal, the consistency of the
correlations from different seasons gives a measure
of the stability and error of the EGFs [*Bensen et al.*,

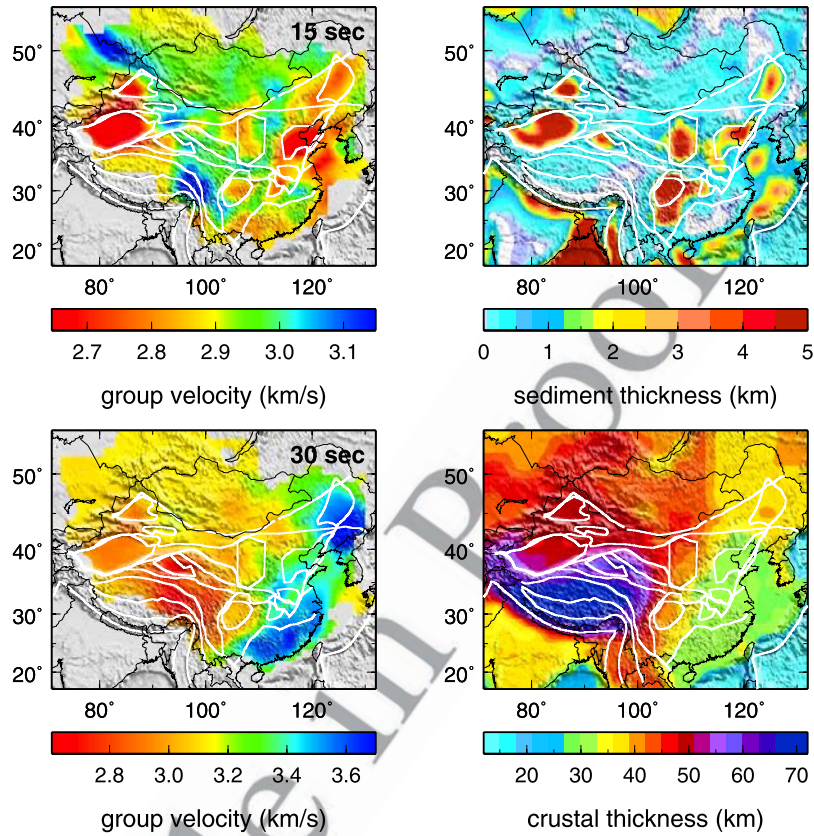


Figure 5. Comparison of group velocities with (top) sediment thickness and (bottom) crustal thickness. Plotted in the background are major block boundaries and basin outlines (Figure 1). (top) The group velocity map (left) is for 15 s Rayleigh waves. The major basins (including Tarim, Junggar, Qadaim, Sichuan, Bohai Wan, and Songliang as well as the southern North China and Jianghang basins in the east central region) are well delineated by slow velocities. See Figure 1 for the locations of the basins. (bottom) The group velocity map is for 30 s Rayleigh waves. The major trend of crust thickening from the east to west (right) is well represented by the velocity decreases from east to west (left).

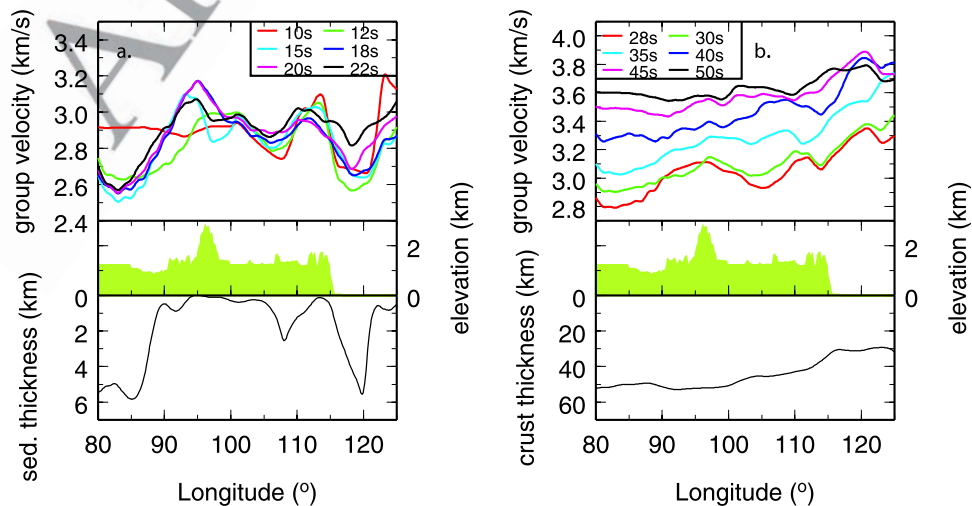


Figure 6. Rayleigh wave group velocities are compared with (a) sediment thickness and (b) crustal thickness along a selected path. The selected path is along the great circle path between (38°N, 80°E) and (38°N, 125°E), passing through three major basins (Tarim, Ordos, and Bohai Wan) (Figure 1). Plotted at the top are velocities (a) for shorter periods and (b) for longer periods. Plotted at the bottom are (a) sediment thickness and (b) crustal thickness. In the middle are surface elevations.

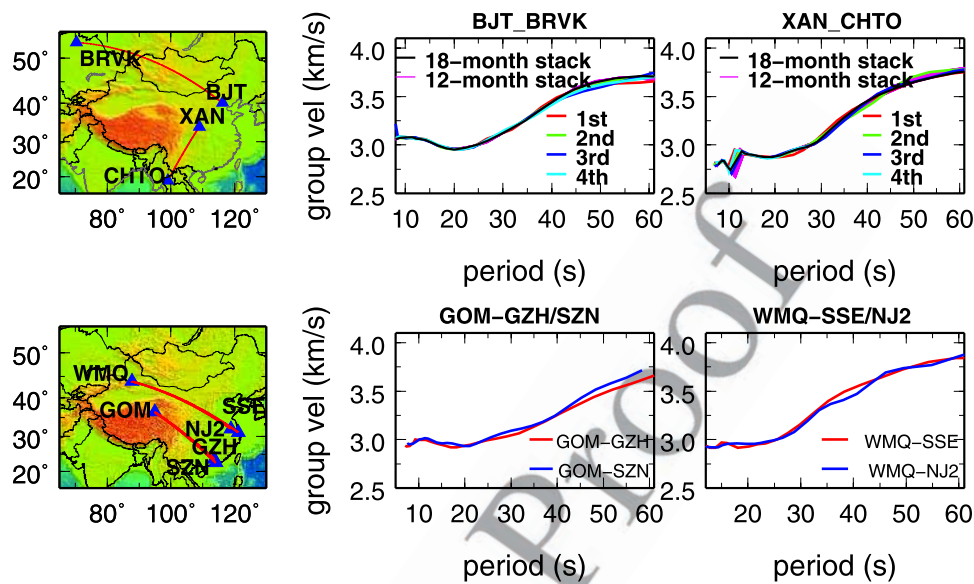


Figure 7. (top) Temporal and (bottom) spatial consistency of dispersion measurements. (top) Comparison of dispersion curves from different time windows. We select two pairs, BJT-BRVK along an east-west path and XAN-CHTO along a north-south path. For each pair, we calculate two sets of EGFs. For each calculation of the EGF, a total of 12 months of data are used. The 18-month stack (including all the data we collected) is plotted for comparison. One set uses seasonal data (red, green, blue, and cyan), i.e., data from the same season over a period of 4 years. The other set uses 12 months of data with a sliding time window of 10 d (total of 19 curves, all in magenta). (bottom) Comparison of dispersion curves between a far-away station and two close stations. We select two pathways, one from GOM to GZH/SZN (distance about 2400 km) and the other from WMQ to SSE/NJ2 (distance about 3100 km). The distance between GZH and SZN is about 133 km, and that between SSE and NJ2 is 245 km.

264 2007]. (4) Spatial consistency: Comparing the EGFs
265 for station-pairs along similar paths [Bensen et al.,
266 2007]. The EGFs between a far-away station to two
267 or more stations that are close to one another
268 should be similar as the paths sample similar
269 structure.

270 [15] We have examined temporal and spatial con-
271 sistency of our dispersion measurements and found
272 that they are very consistent whenever the SNRs of
273 the EGFs are high. Some examples are shown in
274 Figure 7. The temporal comparisons include a
275 station pair with an east-west path (BJT-BRVK)
276 and another pair with a north-south path (XAN-
277 CHTO) (Figure 7, top). We construct 23 dispersion
278 curves using 12-months of data with different
279 sliding windows or using 12-months of data over
280 different seasons. For either pair, we find the
281 standard deviation of these curves to be less than
282 2% for all periods and the standard deviation of the
283 mean to be less than 0.5%. The spatial comparisons
284 include two pathways (Figure 7, bottom), from
285 GOM to GZH/SZN and from WMQ to SSE/NJ2.
286 The group velocities between WMQ and SSE are
287 quite similar to those between WMQ and NJ2 at all
288 the observed periods (10 to 60 s). The group
289 velocities between GOM-GZH and GOM-SZN

are also similar at periods less than 40 s. At periods
greater than 40 s, they are somewhat different but
are within the uncertainties as indicated in the
temporal plots (Figure 7, top). A future effort
will be to quantify systematically the uncertainties
of the dispersion measurements and the velocity
tomography using repeated measurements and
repeated tomography.

Acknowledgments

[16] The CNSN waveform data were provided by China
Earthquake Network Center, and other station data were
obtained from IRIS DMC. We thank reviews from two anonymous
reviewers. One review was particularly constructive and
detailed, which helped improve the paper greatly. The figures
were made using GMT software [Wessel and Smith, 1998]. The
groups at UIUC and CU acknowledge support from Federal
grants AFRL FA8718-07-C-0006, NSF EAR-0330749
(UIUC), and NSF EAR-0337622 (CU).

References

Bensen, G., et al. (2007), Processing seismic ambient noise
data to obtain reliable broad-band surface wave dispersion
measurements, *Geophys. J. Int.*, 169(3), 1239–1260,
doi:10.1111/j.1365-246X.2007.03374.x.



- 314 Bensen, G. D., M. H. Ritzwoller, and N. M. Shapiro (2008),
315 Broadband ambient noise surface wave tomography across the
316 United States, *J. Geophys. Res.*, doi:10.1029/2007JB005248,
317 in press.
- 318 Campillo, M. (2006), Phase and correlation in random seismic
319 fields and the reconstruction of the Green function, *Pure Appl.*
320 *Geophys.*, *163*, 475–502, doi:10.1007/s00024-005-0032-8.
- 321 Campillo, M., and A. Paul (2003), Long-range correlations in
322 the diffuse seismic coda, *Science*, *299*, 547–549, doi:10.1126/
323 science.1078551.
- 324 Curtis, A., et al. (1998), Eurasian fundamental mode
325 surface wave phase velocities and their relationship with
326 tectonic structures, *J. Geophys. Res.*, *103*, 26,919–26,947,
327 doi:10.1029/98JB00903.
- 328 Huang, Z. X., et al. (2003), Rayleigh wave tomography of
329 China and adjacent regions, *J. Geophys. Res.*, *108*(B2),
330 2073, doi:10.1029/2001JB001696.
- 331 Kang, T.-S., and J. S. Shin (2006), Surface-wave tomography
332 from ambient seismic noise of accelerograph networks in
333 southern Korea, *Geophys. Res. Lett.*, *33*, L17303, doi:10.1029/
334 2006GL027044.
- 335 Laske, G., and G. Masters (1997), A global digital map of
336 sediment thickness, *Eos Trans. AGU*, *78*(46), Fall Meet.
337 Suppl., F483.
- 338 Lebedev, S., and G. Nolet (2003), Upper mantle beneath
339 Southeast Asia from S velocity tomography, *J. Geophys.*
340 *Res.*, *108*(B1), 2048, doi:10.1029/2000JB000073.
- 341 Liang, C., and C. A. Langston (2008), Ambient seismic
342 noise tomography and structure of eastern North America,
343 *J. Geophys. Res.*, *113*, B03309, doi:10.1029/2007JB005350.
- 344 Liang, C., X. Song, and J. Huang (2004), Tomographic inver-
345 sion of Pn travel times in China, *J. Geophys. Res.*, *109*,
346 B11304, doi:10.1029/2003JB002789.
- 347 Lin, F., M. P. Moschetti, and M. H. Ritzwoller (2008), Surface
348 wave tomography of the western United States from ambient
349 seismic noise: Rayleigh and Love wave phase velocity
350 maps, *Geophys. J. Int.*, *173*(1), 281–298, doi:10.1111/j.1365-
351 246X.2008.03720.x.
- 352 Lobkis, O. I., and R. L. Weaver (2001), On the emergence of the
353 Greens function in the correlations of a diffuse field, *J. Acoust.*
354 *Soc. Am.*, *110*, 3011–3017, doi:10.1121/1.1417528.
- 355 Paul, A., M. Campillo, L. Margerin, E. Larose, and A. Derode
356 (2005), Empirical synthesis of time-asymmetrical Green
357 functions from the correlation of coda waves, *J. Geophys.*
358 *Res.*, *110*, B08302, doi:10.1029/2004JB003521.
- 359 Ritzwoller, M. H., and A. L. Levshin (1998), Eurasian surface
360 wave tomography: Group velocities, *J. Geophys. Res.*, *103*,
361 4839–4878, doi:10.1029/97JB02622.
- 362 Sabra, K. G., P. Gerstoft, P. Roux, W. A. Kuperman, and M. C.
363 Fehler (2005a), Extracting time domain Green's function
364 estimates from ambient seismic noise, *Geophys. Res. Lett.*,
365 *32*, doi:10.1029/2004GL021862.
- Sabra, K. G., P. Gerstoft, P. Roux, W. A. Kuperman, and M. C. 366
Fehler (2005b), Surface wave tomography from microseisms 367
in Southern California, *Geophys. Res. Lett.*, *32*, L14311, 368
doi:10.1029/2005GL023155. 369
- Shapiro, N. M., and M. Campillo (2004), Emergence of broad- 370
band Rayleigh waves from correlations of the ambient seis- 371
mic noise, *Geophys. Res. Lett.*, *31*, L07614, doi:10.1029/ 372
2004GL019491. 373
- Shapiro, N. M., and M. H. Ritzwoller (2002), Monte-Carlo 374
inversion for a global shear velocity model of the crust and 375
upper mantle, *Geophys. J. Int.*, *151*, 88–105, doi:10.1046/ 376
j.1365-246X.2002.01742.x. 377
- Shapiro, N. M., M. Campillo, L. Stehly, and M. H. Ritzwoller 378
(2005), High resolution surface wave tomography from 379
ambient seismic noise, *Science*, *307*(5715), 1615–1618, 380
doi:10.1126/science.1108339. 381
- Villaseñor, A., Y. Yang, M. H. Ritzwoller, and J. Gallart (2007), 382
Ambient noise surface wave tomography of the Iberian 383
Peninsula: Implications for shallow seismic structure, *Geo-* 384
phys. Res. Lett., *34*, L11304, doi:10.1029/2007GL030164. 385
- Weaver, R. L. (2005), Information from seismic noise, *Science*, 386
307, 1568–1569, doi:10.1126/science.1109834. 387
- Wu, F. T., A. L. Levshin, and V. M. Kozhevnikov (1997), 388
Rayleigh wave group velocity tomography of Siberia, China 389
and the vicinity, *Pure Appl. Geophys.*, *149*, 447–473, 390
doi:10.1007/s000240050035. 391
- Xu, G. M., et al. (2000), The 3-D structure of shear waves in 392
the crust and mantle of east continental China inverted by 393
Rayleigh wave data, *Chin. J. Geophys.*, *43*(3), 395–406. 394
- Yang, Y., and M. H. Ritzwoller (2008), Characteristics of 395
ambient seismic noise as a source for surface wave tomogra- 396
phy, *Geochem. Geophys. Geosyst.*, *9*, Q02008, doi:10.1029/ 397
2007GC001814. 398
- Yang, Y. J., M. H. Ritzwoller, A. L. Levshin, and N. M. Shapiro 399
(2007), Ambient noise Rayleigh wave tomography across 400
Europe, *Geophys. J. Int.*, *168*, 259–274, doi:10.1111/j.1365- 401
246X.2006.03203.x. 402
- Yao, H. J., et al. (2005), Mantle structure from inter-station 403
Rayleigh wave dispersion and its tectonic implication in 404
western China and neighboring regions, *Phys. Earth Planet.* 405
Inter., *148*(1), 39–54, doi:10.1016/j.pepi.2004.08.006. 406
- Yao, H. J., R. D. van der Hilst, and M. V. de Hoop (2006), 407
Surface-wave array tomography in SE Tibet from ambient 408
noise and two-station analysis - I. Phase velocity maps, *Geo-* 409
phys. J. Int., *166*(2), 732–744, doi:10.1111/j.1365-246X. 410
2006.03028.x. 411
- Zhang, Y. S., and T. Lay (1996), Global surface wave phase 412
velocity variations, *J. Geophys. Res.*, *101*, 8415–8436, 413
doi:10.1029/96JB00167. 414
- Zhu, J. S., et al. (2002), High resolution surface wave tomo- 415
graphy in East Asia and West Pacific marginal seas, *Chin. J.* 416
Geophys., *45*(5), 679–698. 417